



# Unbounded Foundation Effects on Seismic Responses of Structures with Passive Control

C. S. Tsai

Associate Professor, Department of Civil Engineering,  
Feng Chia University, Taichung, Taiwan, R. O. C.

C. S. Chen

S. B. Lin

Graduate Students, Department of Civil Engineering,  
Feng Chia University, Taichung, Taiwan, R. O. C.

W. S. Pong

Assistant Professor, School of Engineering,  
San Francisco State University, San Francisco, California, U. S. A.

## ABSTRACT

Fluid viscous dampers can provide additional damping to improve the seismic resistibility of a structure. In the past, a lot of efforts have been made to investigate the seismic behavior of structures with fluid dampers by neglecting the foundation-structure interaction effects. In order to ensure the safety of structures, it is demanded to apprehend the interactive behavior of damped structures and unbounded foundation during earthquakes. Presented in this paper is rigorous a time-domain procedure to address the interaction effects of structures equipped with fluid viscous dampers and the foundation with an unbounded medium. Numerical results reveal that there exist significant differences between the system with and without the radiation damping during earthquakes. It is also implied from this study that to yield better accuracy, the radiation damping should be properly taken into account. Moreover, the efficiency of fluid viscous dampers in reducing seismic disturbance of a structure is very dependent on the flexibility of the foundation.

## INTRODUCTION

Many passive control devices have been recognized

as effective tools in improving seismic resistance of structures. The use of supplemental fluid viscous dampers to dissipate the seismic energy is considered to be one of the most economic and effective ways to mitigate the effects of earthquakes on structures. Fluid viscous damping devices originated in the early 1960's for use in steel mills as energy absorbing buffers on overhead cranes. Recently, fluid viscous dampers (Constantinou, et al 1990[1]), as shown in Fig. 1, have been adopted for some large scale applications. Its linear viscous behavior and independence over a wide temperature range ( $-40^{\circ}\text{C}$  to  $70^{\circ}\text{C}$ ) are the two major characteristics of interest in applications of seismic study. However, the behavior of soil-structure interaction during the excitation of earthquakes is quite complicated even the structure equipped with fluid viscous dampers. It is required to know the interactive behavior of structures equipped with fluid viscous dampers and unbounded foundation during earthquakes. Unfortunately, the radiation problem resulted from the unbounded soil remains unsolved. In the last twenty years, significant advances have been made in this area. Most notable developments of the procedures are based on boundary-integral or boundary-element methods for unbounded media. Nonetheless, a major need still exists for alternative approaches, particularly for procedures that could be implemented within the context

of finite element analyses. These procedures would be more familiar to structural analyses, and would allow greater flexibility in terms of the geometrical and material characterization of the unbounded medium. In this paper, a new time-domain procedure, based on the finite element method, the semi-analytical solution and the infinitesimal finite-element cell method, has been presented to address the interactive behavior of structures equipped with fluid viscous dampers and foundation with an unbounded region (Fig. 2). To yield more accurate results, a time domain procedure in virtue of similarity theory has been developed to simulate the radiation features of the infinite domain (Tsai et al. 1999a[2], 1999b[3], 1999c[4]). The probes into the influence and discussions to the seismic behavior of structures equipped with fluid viscous dampers on different foundations have been examined.

#### TIME-DOMAIN SUBSTRUCTURE METHOD FOR STRUCTURE EQUIPPED WITH FLUID VISCOUS DAMPERS AND UNBOUNDED MEDIA

The substructure method is adopted for the analysis of the interested system. As shown in Fig. 2, the entire system is divided into three substructures including the building, foundation and fluid viscous dampers. Furthermore, the soil medium is also divided into two regions: the near and the far field of the soil. The far field of the soil extends to infinity. For the dynamic analysis of the structure equipped with fluid viscous dampers and unbounded media, the structure, fluid viscous dampers and the near field of the soil can be discretized by using the finite element method (see Fig. 3).

#### EQUATIONS OF MOTION OF BUILDING AND NEAR FIELD OF FOUNDATION

As depicted in Figs. 2 and 3, the structure, fluid viscous damper and the near field of the soil can be discretized by the finite element method. The equation of motion of the structure and the near field of the foundation is given by:

$$\mathbf{M}\ddot{\mathbf{U}}(t) + \mathbf{C}\dot{\mathbf{U}}(t) + \mathbf{K}\mathbf{U}(t) = -\mathbf{M}\mathbf{B}\ddot{\mathbf{u}}_g(t) + \mathbf{Q}(t) \quad (1)$$

$\mathbf{M}$ ,  $\mathbf{C}$ ,  $\mathbf{K}$  = symmetrical mass, damping, and stiffness matrices, respectively, for the building and the near field of the foundation.  $\mathbf{U}(t)$ ,  $\dot{\mathbf{U}}(t)$ ,  $\ddot{\mathbf{U}}(t)$  = vectors of nodal displacements, velocities, and accelerations relative to the ground, respectively;  $\ddot{\mathbf{u}}_g(t)$  = ground motion;  $\mathbf{B}$  = displacement transformation matrix; and  $\mathbf{Q}(t)$  = vector of dynamic forces resulting from the far field of the foundation.

#### ANALYTICAL MODEL FOR FLUID VISCOUS DAMPER

The fluid damper exhibits viscoelastic fluid behavior over a large frequency. The simplest model to simulate the mechanical behavior of the fluid viscous damper is the Maxwell model (Bird et al. 1987[5]) given by:

$$P(t) + \lambda \dot{P}(t) = C_0 \dot{U}(t) \quad (2)$$

where  $\lambda$  is the relaxation time,  $C_0$  is the damping constant at zero frequency,  $P(t)$  is the force acting on the fluid damper,  $\dot{U}(t)$  is the damper position velocity.

A more general Maxwell model may also be considered where the derivatives are of fractional order (Markris et al. 1991[6]):

$$P(t) + \lambda D^r P(t) = C_0 D^q U(t) \quad (3)$$

where  $D^r f(t)$  is the fractional derivative of order  $r$  of the time depend function  $f$ . Eq.(3) may provide better results than Eq.(2) in simulating the mechanical behavior of complex fluid dampers. Due to the assumption that the damping coefficient is independent of the velocity over a wide range of values, the parameter  $q$  can be set equal to 1, the parameter  $C_0$  is the damping constant at zero frequency. If  $r$  is also set equal to one, Eq.(3) is equal to Eq.(2).

For convenience, mathematical models for fluid dampers should be easily implemented in computer programs to facilitate their use in engineering practice. For this reason, a finite element formulation for the fluid dampers is developed. The global coordinate system  $x$ ,  $y$ , and  $z$ , and the local coordinate system  $\xi$ ,  $\zeta$ , and  $\eta$ , are depicted in Fig. 4. The global displacements at nodal points 1 and 2 shown in Fig. 4 are  $\mathbf{D}_1(t)$  and  $\mathbf{D}_2(t)$ , respectively. These global displacements can be expressed as:

$$\mathbf{D}_1(t) = \begin{bmatrix} u_{1x}(t) \\ u_{1y}(t) \\ u_{1z}(t) \end{bmatrix} \quad (4)$$

and

$$\mathbf{D}_2(t) = \begin{bmatrix} u_{2x}(t) \\ u_{2y}(t) \\ u_{2z}(t) \end{bmatrix} \quad (5)$$

where  $u_{1x}(t)$ ,  $u_{1y}(t)$ , and  $u_{1z}(t)$  are global displacement at nodal point in the  $x$ ,  $y$ , and  $z$  directions, respectively, and  $u_{2x}(t)$ ,  $u_{2y}(t)$ , and  $u_{2z}(t)$  are those at nodal point 2, respectively.

The local displacements  $\bar{\mathbf{D}}_1(t)$  and  $\bar{\mathbf{D}}_2(t)$  at nodal points 1 and 2, respectively, as shown in Fig. 4, can be expressed in terms of global displacements as:

$$\bar{\mathbf{D}}_1(t) = \mathbf{R}\mathbf{D}_1(t) \quad (6)$$

$$\bar{\mathbf{D}}_2(t) = \mathbf{R}\mathbf{D}_2(t) \quad (7)$$

where  $\mathbf{R}$  is the transformation matrix between the global and local coordinate systems. The relative displacement  $\bar{\mathbf{U}}(t)$  between nodal points 1 and 2 in the local coordinate system can be defined as:

$$\bar{\mathbf{U}}(t) = \bar{\mathbf{D}}_2(t) - \bar{\mathbf{D}}_1(t) = \mathbf{R}\mathbf{D}_2(t) - \mathbf{R}\mathbf{D}_1(t) = \bar{\mathbf{B}} \begin{Bmatrix} \mathbf{D}_1(t) \\ \mathbf{D}_2(t) \end{Bmatrix} = \bar{\mathbf{B}}\mathbf{U}(t) \quad (8)$$

where

$$\bar{\mathbf{B}} = \begin{bmatrix} -\mathbf{R} & \mathbf{R} \end{bmatrix} \quad (9)$$

$$\mathbf{U}(t) = \begin{bmatrix} \mathbf{D}_1(t) \\ \mathbf{D}_2(t) \end{bmatrix} = \begin{bmatrix} u_{1x}(t) \\ u_{1y}(t) \\ u_{1z}(t) \\ u_{2x}(t) \\ u_{2y}(t) \\ u_{2z}(t) \end{bmatrix} \quad (10)$$

and

$$\bar{\mathbf{U}}(t) = \begin{bmatrix} \mathbf{U}_\zeta(t) \\ \mathbf{U}_\eta(t) \\ \mathbf{U}_\gamma(t) \end{bmatrix} \quad (11)$$

Therefore, the relative velocity  $\dot{\bar{\mathbf{U}}}(t)$  between nodal points 1 and 2 in the local coordinate system is given by:

$$\dot{\bar{\mathbf{U}}}(t) = \frac{\partial \bar{\mathbf{U}}(t)}{\partial t} = \bar{\mathbf{B}} \frac{\partial \mathbf{U}(t)}{\partial t} = \bar{\mathbf{B}} \begin{bmatrix} \frac{\partial \mathbf{D}_1(t)}{\partial t} \\ \frac{\partial \mathbf{D}_2(t)}{\partial t} \end{bmatrix} \quad (12)$$

As a result

$$\dot{\bar{\mathbf{U}}}(t) = \bar{\mathbf{B}}\dot{\mathbf{U}} = \bar{\mathbf{B}} \begin{bmatrix} \dot{u}_{1x}(t) \\ \dot{u}_{1y}(t) \\ \dot{u}_{1z}(t) \\ \dot{u}_{2x}(t) \\ \dot{u}_{2y}(t) \\ \dot{u}_{2z}(t) \end{bmatrix} \quad (13)$$

The model for fluid dampers is

$$\mathbf{P}(t) + \lambda \dot{\mathbf{P}}(t) = C_0 \dot{\bar{\mathbf{U}}}(t) \quad (14)$$

If linear variation between two arbitrary time steps,  $(n-1)\Delta t$  and  $n\Delta t$ , is assumed, then the order one fractional derivation of the damping force can be expressed as

$$\dot{\mathbf{P}}(t) = \frac{\mathbf{P}_n(t) - \mathbf{P}_{n-1}(t)}{\Delta t} = \frac{\mathbf{P}(t) - \mathbf{P}_{n-1}(t)}{\Delta t} \quad (15)$$

Then Eq.(14) can be rewritten as

$$\mathbf{P}(t) + \frac{\lambda}{\Delta t} (\mathbf{P}(t) - \mathbf{P}_{n-1}(t)) = C_0 \dot{\bar{\mathbf{U}}}(t) \quad (16)$$

Rearranging Eq.(16), one obtains

$$\mathbf{P}(t) = \frac{C_0}{1 + \frac{\lambda}{\Delta t}} \dot{\bar{\mathbf{U}}}(t) + \frac{\lambda}{\Delta t} \frac{1}{1 + \frac{\lambda}{\Delta t}} \mathbf{P}_{n-1}(t) \quad (17)$$

Substitution of Eq.(13) into Eq.(17) yields

$$\mathbf{P}(t) = \frac{C_0}{1 + \frac{\lambda}{\Delta t}} \bar{\mathbf{B}}\dot{\mathbf{U}}(t) + \frac{\lambda}{\Delta t} \frac{1}{1 + \frac{\lambda}{\Delta t}} \mathbf{P}_{n-1}(t) \quad (18)$$

Using the virtual work principle, the equivalent nodal forces  $\mathbf{F}(t)$  can be obtained as

$$\begin{aligned} \mathbf{F}(t) &= \bar{\mathbf{B}}^T \mathbf{P}(t) = \frac{C_0}{1 + \frac{\lambda}{\Delta t}} \bar{\mathbf{B}}^T \bar{\mathbf{B}} \dot{\mathbf{U}}(t) + \frac{\lambda}{\Delta t} \frac{1}{1 + \frac{\lambda}{\Delta t}} \bar{\mathbf{B}}^T \mathbf{P}_{n-1}(t) \\ &= \mathbf{C}_f \dot{\mathbf{U}}(t) + \frac{\lambda}{\Delta t} \frac{1}{1 + \frac{\lambda}{\Delta t}} \bar{\mathbf{B}}^T \mathbf{P}_{n-1}(t) \end{aligned} \quad (19)$$

where the matrix  $\mathbf{C}_f$  is the added damping resulting from fluid dampers:

$$\mathbf{C}_f = \frac{C_0}{1 + \frac{\lambda}{\Delta t}} \bar{\mathbf{B}}^T \bar{\mathbf{B}} \quad (20)$$

## SYSTEM EQUATIONS FOR FAR FIELD OF FOUNDATION

As shown in Fig. 2, the foundation medium is divided into two regions: the near and far fields of the foundation. The far field of the foundation extends to infinity. Adopting the similarity theorem, as shown in Fig. 5, Wolf and Song developed the consistent infinitesimal finite-element cell method accounting for the radiation damping for the unbounded medium in the time domain (Song and Wolf 1995[7], 1996a[8], 1996b[9]; Wolf and Song 1996[10]). The governing equation of the far field of foundation can be expressed as:

$$\mathbf{I}(t) = \int_0^t \mathbf{M}^\infty(t - \tau) \ddot{\mathbf{U}}(\tau) d\tau \quad (21)$$

$\mathbf{I}(t)$  is the interaction forces at the interface of the near and far fields of the unbounded medium and  $\mathbf{M}^\infty(t)$  is the acceleration unit-impulse response matrix in the time domain. The relation of the vector of dynamic forces from the far field  $\mathbf{I}(t)$  to those acting on the near field  $\mathbf{Q}(t)$  is

$$\mathbf{Q}(t) = -\mathbf{I}(t) \quad (22)$$

As shown in Fig. 6, owing to similarity, the coordinates of the nodes on the exterior boundary can be expressed by those of the nodes on the interior boundary and the dimensionless cell width  $w$

$$y_4 = (1+w)y_1, \quad y_5 = (1+w)y_2, \quad y_6 = (1+w)y_3 \quad (23a)$$

$$z_4 = (1+w)z_1, \quad z_5 = (1+w)z_2, \quad z_6 = (1+w)z_3 \quad (23b)$$

The nodes on the interior boundary are identified by subscripts 1, 2, 3 and the nodes on the exterior boundary are identified by subscripts 4, 5, 6, respectively. The cell width  $w$  can be expressed as  $w = (r_e - r_i)/r_i$  and

$$\mathbf{Y}_e = (1+w)\mathbf{Y}_i, \quad \mathbf{Z}_e = (1+w)\mathbf{Z}_i \quad (24)$$

Note that the subscript  $i$  and  $e$  portray the interior boundary and the exterior boundary, respectively.  $\mathbf{Y}_e$  and  $\mathbf{Z}_e$  denote the coordinates of the nodes on the exterior boundary.  $\mathbf{Y}_i$  and  $\mathbf{Z}_i$  indicate the coordinates of the nodes on the interior boundary. The shape function matrix of the finite element is

$$\hat{\mathbf{N}} = [\mathbf{N}_i \quad \mathbf{N}_e] \quad (25)$$

and

$$\mathbf{N}_j = \frac{1}{2}(1 - \xi_j \xi) \mathbf{N}, \quad (j = i, e) \quad (26)$$

where  $\xi_i = -1$  and  $\xi_e = 1$ .  $\mathbf{N}$  = the shape function vector in the  $\eta$  direction. Therefore, the stiffness matrix of the finite element equals

$$\mathbf{K}_{jl} = \int_S \mathbf{B}_j^T \mathbf{D} \mathbf{B}_l dS = \int_{-1}^{+1} \int_{-1}^{+1} \mathbf{B}_j^T \mathbf{D} \mathbf{B}_l |\hat{\mathbf{J}}| d\xi d\eta \quad (27)$$

,  $(j = i, e; l = i, e)$

The Jacobian matrix of a particular element equals

$$\hat{\mathbf{J}} = \begin{bmatrix} Y_{,\xi} & Z_{,\xi} \\ Y_{,\eta} & Z_{,\eta} \end{bmatrix} = \begin{bmatrix} \frac{w}{2} & 0 \\ 0 & 1 + \frac{w}{2}(1 + \xi) \end{bmatrix} \mathbf{J} \quad (28)$$

where

$$\mathbf{J} = \begin{bmatrix} \mathbf{N} \mathbf{Y}_i & \mathbf{N} \mathbf{Z}_i \\ \mathbf{N}_{,\eta} \mathbf{Y}_i & \mathbf{N}_{,\eta} \mathbf{Z}_i \end{bmatrix} \quad (29)$$

The determinant of the Jacobian matrix is given by:

$$|\hat{\mathbf{J}}| = \frac{w}{2} \left( 1 + \frac{w}{2}(1 + \xi) \right) |\mathbf{J}| \quad (30)$$

where  $\mathbf{J}^{-1}$  is denoted as

$$\mathbf{J}^{-1} = \begin{bmatrix} j_{11} & j_{12} \\ j_{21} & j_{22} \end{bmatrix} \quad (31)$$

The strain-nodal displacement matrix is

$$\mathbf{B} = [\mathbf{B}_i \quad \mathbf{B}_e] \quad (32)$$

$$\mathbf{B}_{jk} = \frac{\xi_j}{w} \mathbf{B}_k^1 + \frac{1 + \xi_j \xi}{2 \left( 1 + \frac{w}{2}(1 + \xi) \right)} \mathbf{B}_k^2 \quad (33)$$

,  $(j = i, e; k = 1, 2, \dots)$

and

$$\mathbf{B}_k^1 = \begin{bmatrix} j_{11} & 0 \\ 0 & j_{21} \\ j_{21} & j_{11} \end{bmatrix} N_k, \quad \mathbf{B}_k^2 = \begin{bmatrix} j_{12} & 0 \\ 0 & j_{22} \\ j_{22} & j_{12} \end{bmatrix} N_k, \quad (34)$$

,  $(k = 1, 2, \dots)$

$N_k$  = the shape function at nodal point  $k$ . Substituting Eq.(30) and Eq.(33) in Eq.(27) yields

$$\mathbf{K}_{jl} = \frac{1}{w} \mathbf{K}_{jl}^0 + \mathbf{K}_{jl}^1 + w \mathbf{K}_{jl}^2, \quad (j = i, e; l = i, e) \quad (35)$$

where

$$\mathbf{K}_{jl}^0 = \xi_j \xi_l \mathbf{E}^0 \quad (36a)$$

$$\mathbf{K}_{jl}^1 = \frac{\xi_j \xi_l}{2} \mathbf{E}^0 + \frac{\xi_l}{2} \mathbf{E}^1 + \frac{\xi_j}{2} (\mathbf{E}^1)^T \quad (36b)$$

$$\mathbf{K}_{jl}^2 = \left( \frac{\xi_l}{4} + \frac{\xi_j \xi_l}{12} \right) \mathbf{E}^2 \quad (36c)$$

and

$$\mathbf{E}^0 = \int_{-1}^{+1} (\mathbf{B}^1)^T \mathbf{D} \mathbf{B}^1 |\mathbf{J}| d\eta \quad (37a)$$

$$\mathbf{E}^1 = \int_{-1}^{+1} (\mathbf{B}^2)^T \mathbf{D} \mathbf{B}^1 |\mathbf{J}| d\eta \quad (37b)$$

$$\mathbf{E}^2 = \int_{-1}^{+1} (\mathbf{B}^2)^T \mathbf{D} \mathbf{B}^2 |\mathbf{J}| d\eta \quad (37c)$$

The detail is referred to Song and Wolf 1995[7], 1996a[8], and 1996b[9]; Wolf and Song 1996[10]. The final form of the consistent infinitesimal finite-element cell equation in the time domain is given by

$$\int_0^t [\mathbf{m}^\infty(t - \tau)] [\mathbf{m}^\infty(\tau)] d\tau + \mathbf{e}^1 \int_0^t \int_0^\tau [\mathbf{m}^\infty(\tau')] d\tau' d\tau + \int_0^t \int_0^\tau [\mathbf{m}^\infty(\tau')] d\tau' d\tau (\mathbf{e}^1)^T + t \int_0^t [\mathbf{m}^\infty(t - \tau)] d\tau - \frac{t^3}{6} \mathbf{e}^2 H(t) - t \mathbf{m}^0 H(t) = 0 \quad (38)$$

where

$$\mathbf{m}^\infty(\tau) = (\mathbf{V}^{-1})^T \mathbf{M}^\infty(\tau) \mathbf{V}^{-1} \quad (39a)$$

$$\mathbf{E}^0 = \mathbf{V}^T \mathbf{V} \quad (39b)$$

$$\mathbf{e}^1 = (\mathbf{V}^{-1})^T \mathbf{E}^1 \mathbf{V}^{-1} - \frac{3}{2} \mathbf{I} \quad (39c)$$

$$\mathbf{e}^2 = (\mathbf{V}^{-1})^T \left[ \mathbf{E}^2 - \mathbf{E}^1 (\mathbf{E}^0)^{-1} (\mathbf{E}^1)^T \right] \mathbf{V}^{-1} \quad (39d)$$

$$\mathbf{m}^0 = (\mathbf{V}^{-1})^T \mathbf{M}^0 \mathbf{V}^{-1} \quad (39e)$$

$$\mathbf{M}^0 = \int_{-1}^{+1} \rho \mathbf{N}^T \mathbf{N} |\mathbf{J}| d\eta \quad (39f)$$

$\rho$  = mass density. After determining  $\mathbf{m}^\infty(\tau)$  from Eq.(38), the acceleration unit-impulse response matrix may be written as

$$\mathbf{M}^\infty(\tau) = \mathbf{V}^T \mathbf{m}^\infty(\tau) \mathbf{V} \quad (40)$$

The entire history of time is divided into  $n$  equal intervals  $\Delta t$ . It is assumed that matrix  $\mathbf{M}^\infty(\tau)$  and the acceleration is piece-wise constant over each time step

$$\ddot{\mathbf{U}}(\tau) = \frac{1}{2} \left\{ \ddot{\mathbf{U}}[(n-1)\Delta t] + \ddot{\mathbf{U}}(n\Delta t) \right\}, \quad (n-1)\Delta t \leq \tau \leq n\Delta t \quad (41)$$

With the aid of Eq.(41),  $\mathbf{I}(t)$  of Eq.(21) can be expressed as:

$$\begin{aligned} \mathbf{I}(t) &= \int_0^t [\mathbf{M}^\infty(t-\tau)] \ddot{\mathbf{U}}(\tau) d\tau = \int_0^t [\mathbf{M}^\infty(\tau)] [\ddot{\mathbf{U}}(t-\tau)] d\tau \\ &= \frac{\Delta t}{2} \sum_{n=2}^N \mathbf{M}^\infty \left[ \left( n - \frac{1}{2} \right) \Delta t \right] \left\{ \ddot{\mathbf{U}}[(N-n+1)\Delta t] + \ddot{\mathbf{U}}[(N-n)\Delta t] \right\} \\ &+ \frac{\Delta t}{2} \mathbf{M}^\infty \left( \frac{\Delta t}{2} \right) \left\{ \ddot{\mathbf{U}}[(N-1)\Delta t] \right\} + \frac{\Delta t}{2} \mathbf{M}^\infty \left( \frac{\Delta t}{2} \right) [\ddot{\mathbf{U}}(N\Delta t)] \\ &= \bar{\mathbf{M}} \ddot{\mathbf{U}}(N\Delta t) + \bar{\mathbf{F}} \end{aligned} \quad (42)$$

where

$$\bar{\mathbf{M}} = \frac{\Delta t}{2} \left[ \mathbf{M}^\infty \left( \frac{\Delta t}{2} \right) \right] \quad (43)$$

$$\begin{aligned} \bar{\mathbf{F}} &= \frac{\Delta t}{2} \sum_{n=2}^N \mathbf{M}^\infty \left[ \left( n - \frac{1}{2} \right) \Delta t \right] \left\{ \ddot{\mathbf{U}}[(N-n+1)\Delta t] + \ddot{\mathbf{U}}[(N-n)\Delta t] \right\} \\ &+ \frac{\Delta t}{2} \left[ \mathbf{M}^\infty \left( \frac{\Delta t}{2} \right) \right] \left\{ \ddot{\mathbf{U}}[(N-1)\Delta t] \right\} \end{aligned} \quad (44)$$

### TIME—DOMAIN FINITE ELEMENT METHOD FOR STRUCTURE EQUIPPED WITH FLUID VISCOUS DAMPERS AND UNBOUNDED MEDIA

Substituting Eq.(22) and Eq.(42) into Eq.(1) results in

$$(\mathbf{M} + \bar{\mathbf{M}}) \ddot{\mathbf{U}}(t) + \mathbf{C} \dot{\mathbf{U}}(t) + \mathbf{K} \mathbf{U}(t) = -\mathbf{M} \ddot{\mathbf{u}}_g(t) - \bar{\mathbf{F}}(t) \quad (45)$$

$\bar{\mathbf{M}}$  is an added mass from the far field acting on the near field of the foundation.  $\bar{\mathbf{F}}(t)$  is an added-load matrix representing the previous time effect. Applying the

Newmark method to Eq.(45), at the  $N$ th time step, we have

$$\hat{\mathbf{K}} \mathbf{U}^N = \hat{\mathbf{R}}^N \quad (46)$$

where

$$\hat{\mathbf{K}} = \mathbf{K} + a_0 (\mathbf{M} + \bar{\mathbf{M}}) + a_1 \mathbf{C} \quad (47)$$

$$\begin{aligned} \hat{\mathbf{R}}^N &= -\mathbf{M} \ddot{\mathbf{u}}_g^N \\ &+ (\mathbf{M} + \bar{\mathbf{M}}) (a_0 \mathbf{U}^{N-1} + a_2 \dot{\mathbf{U}}^{N-1} + a_3 \ddot{\mathbf{U}}^{N-1}) \\ &+ \mathbf{C} (a_1 \mathbf{U}^{N-1} + a_4 \dot{\mathbf{U}}^{N-1} + a_5 \ddot{\mathbf{U}}^{N-1}) - \bar{\mathbf{F}} \end{aligned} \quad (48)$$

where  $a_0 = 1/\alpha \Delta t^2$ ;  $a_1 = \delta/\alpha \Delta t$ ;  $a_2 = 1/\alpha \Delta t$ ;  $a_3 = (1/2\alpha) -$ ;  $a_4 = (\delta/\alpha) -$ ;  $a_5 = (\Delta t/2)[(\delta/\alpha) - 2]$ ;  $\delta \geq 0.50$ ;  $\alpha \geq 0.25(0.5 + \delta)^2$ .

The numerical methods described in this paper have been installed in the computer program "NSAT" (Tsai 1996[11]).

### NUMERICAL EXAMPLES

To ensure the safety of structures, it essential to know the interactive behavior of the building equipped with fluid viscous dampers and foundation with an unbounded region during earthquakes. For this purpose, a 10-story building equipped with fluid viscous dampers, as shown in Fig. 2, is given as an example to study the influence of different elastic moduli of the foundation on the seismic responses of building equipped with fluid viscous dampers. A detail description of the 10-story building is shown in Fig. 7. The material used for the building has Poisson's ratio and elastic modulus equal to 0.3 and 200 GPa, respectively. The weight for each floor is 4460.6N/m. The radius of the near field of the soil below the building is around the 249m. The Poisson's ratio of the stratum is 0.3 and the weight density is 1.8 KN/m<sup>3</sup>.

It was assumed that the floors were rigid in their own plane in numerical analysis. The damping constant  $C_0$  of fluid viscous damper is 525.59 KN·s/m and the whole system was subjected to 1940 El Centro earthquake ground motion. Fig. 8 and 9 show the relative displacement responses at points A and B (as shown in Fig.1) when the building equipped with fluid viscous dampers during earthquakes. Fig. 10 and 11 show the shear force responses at point B (see Fig. 1) when the building equipped with fluid viscous dampers during earthquakes. In these figures, the bold-solid line is the seismic response of the building on rigid foundation (without soil) and the dotted line is the response of the building on the flexible foundation with radiation damping during earthquakes. With reference to Fig. 8 to Fig. 11, it

indicates that the seismic responses of the building have remarkable differences on different foundations. When the elastic moduli of the near field of foundation are different, the comparisons of the maximum relative displacement responses at points A and B of the building equipped with fluid viscous dampers on the unbounded soil are shown in Fig. 12 and Fig. 13. Figs. 14 and 15 shows the comparisons of the maximum shear force responses at point B when the building equipped with fluid viscous dampers on the unbounded soil. With reference to Fig. 12 to Fig. 15, there exist significant differences between the responses of the building on different foundations during earthquakes. It also reveals that the whole system becomes more flexible due to the involvement of the foundation and that the effectiveness of the fluid viscous damper in reducing seismic responses of the building is considerably downgraded.

## CONCLUSIONS

Fluid viscous damper has been recognized as an effective tool for improving seismic resistance of structures. Nevertheless, soil-structure interaction is a very complicated behavior. To ensure the safety of structures, it necessitates knowing the interactive behavior of the structure and foundation during earthquakes, even the structure is equipped with fluid viscous dampers. It also should be considered the effects of the radiation damping and the flexibility from the soil media. Numerical results show that there exist remarkable differences for the seismic behavior of the system with and without flexible foundation. It is illustrated from this study that to obtain better accuracy, the radiation damping should be properly taken into account. It is also exhibited that interaction effects are important between the building equipped with fluid viscous dampers and the unbounded soil medium and that it may cause structure damage without considering the influence from the flexible foundation.

## APPENDIX. REFERENCES

[1] Constantinou, M. C. and Hanson, R. D. (1990). "Viscoelastic versus steel plate mechanical damping devices : An experimental comparison." *Proc. 4th U.S. Nat. Conf. On Earthq. Engng., Earthq. Engng. Res. Institute, Oakland, California*, Vol. III, 469-477.

[2] Tsai, C. S. and Chen, C. S. (1999a). "Interactive behavior for isolated building with FPS and unbounded media during earthquakes." *Asian-Pacific Symposium on Structural Reliability and its Applications, Taipei, Taiwan, R. O. C.*, in press.

[3] Tsai, C. S., Chen, C. S., Lin, S. B. and Chen, B. J. (1999b). "Seismic behavior of dam-reservoir-foundation and unbounded media." *ASME/JSME PVP Conference, Boston, U.S.A.*, in press.

[4] Tsai, C. S., Chen, C. S., Chen, B. J. and Lin, S. B. (1999c). "Interactive behavior of damped structures and unbounded media." *ASME/JSME PVP Conference, Boston, U.S.A.*, in press.

[5] Bird, R. B., Armstrong, R. C. and Hassager, O. (1987). "Dynamics of polymeric liquids." *J. Wiley and Sons, New York*.

[6] Markris, N. and Constantinou, M. C. (1991). "Fractional derivative Maxwell model for viscous dampers." *J. Struct. Engrg.*, ASCE, 117(9), 2708-2724.

[7] Ch. Song and J. P. Wolf (1995), "Consistent infinitesimal finite-element cell method: out-of-plane motion." *J. Engrg. Mech.*, ASCE, 121, 613-619.

[8] Ch. Song and J. P. Wolf (1996a), "Consistent infinitesimal finite-element cell method: three-dimensional vector wave equation." *Int. J. Numerical. Methods in Engrg.*, 39, 2189-2208.

[9] Ch. Song and J. P. Wolf (1996b), "Consistent infinitesimal finite-element cell method for diffusion equation in unbounded medium." *Computer Methods in Applied Mechanics and Engineering*, 132, 319-334.

[10] J. P. Wolf and Ch. Song (1996), "Consistent infinitesimal finite-element cell method: three-dimensional scalar wave equation" *J. Applied. Mech.*, ASME, 63, 650-654.

[11] C. S. Tsai (1996), "Nonlinear Stress Analysis Techniques. - NSAT " *Department of Civil Engineering, Feng Chia University, Taichung Taiwan, R.O.C.*

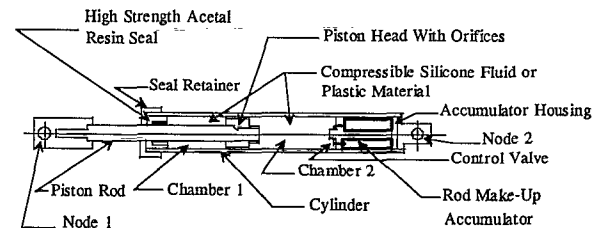


Fig. 1 Construction of Fluid Damper

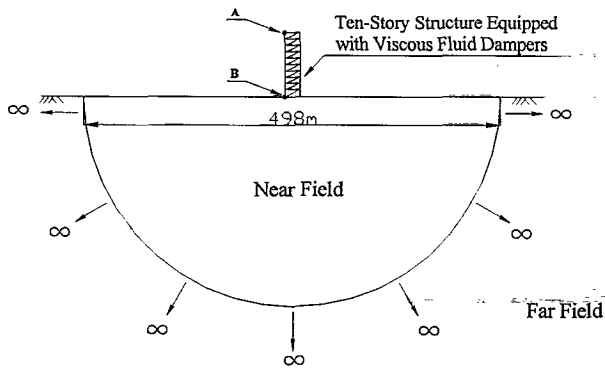


Fig. 2 10-Story Building Equipped with Fluid Viscous Dampers and Foundation

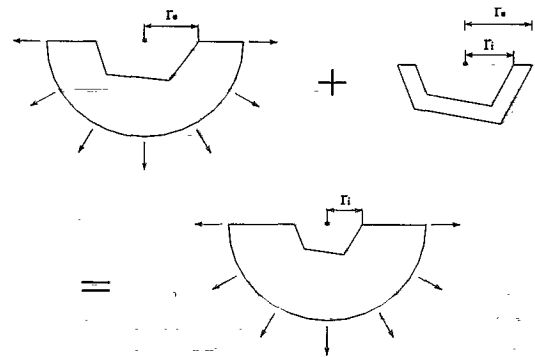


Fig. 5 Fundamental Concept of Consistent Infinitesimal Finite-Element Cell Method

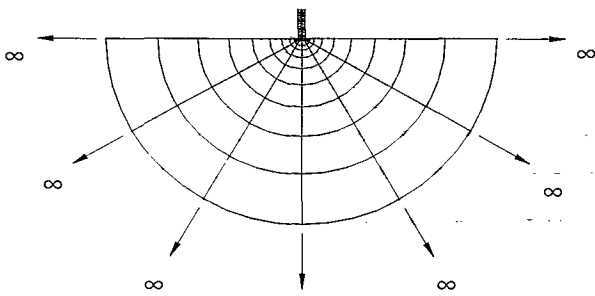


Fig. 3 Finite Element Mesh for Building Equipped with Fluid Viscous Damper and Foundation

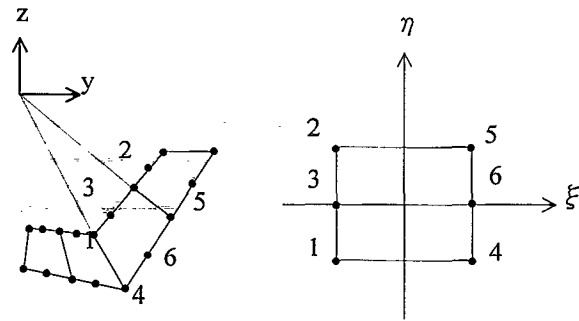


Fig. 6 Two-dimensional Finite-Element Cell and Parent Element on Discretized Interface

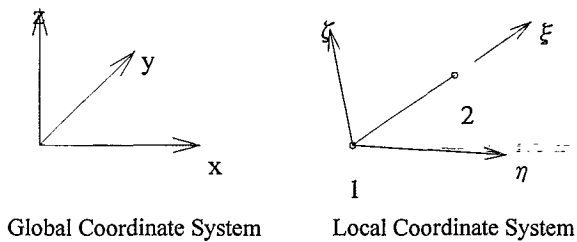


Fig. 4 Two Node Element

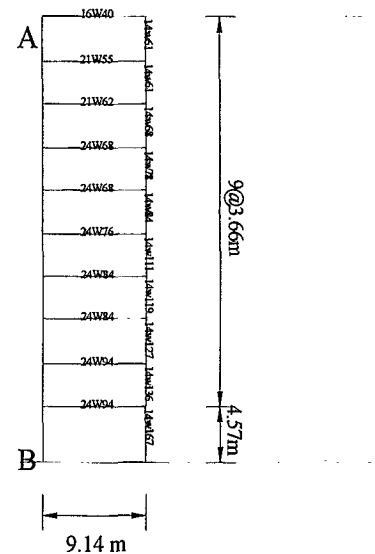


Fig. 7 A 10-story Building Frame

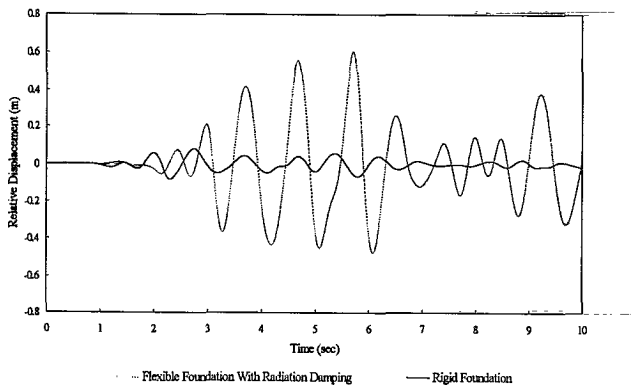


Fig. 8 Comparison of Relative Displacements between Points A and B while Elastic Modulus of Far Field is  $1.0 \times 10^7$  KN/m<sup>2</sup> and Elastic Modulus of Near Field is  $1.0 \times 10^5$  KN/m<sup>2</sup>

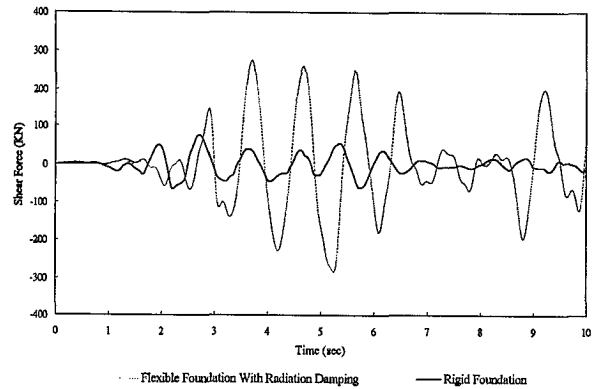


Fig. 10 Comparison of Shear Forces at Point B while Elastic Modulus of Far Field is  $1.0 \times 10^7$  KN/m<sup>2</sup> and Elastic Modulus of Near Field is  $1.0 \times 10^5$  KN/m<sup>2</sup>

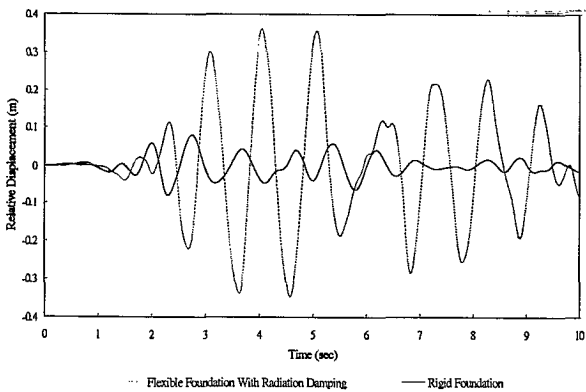


Fig. 9 Comparison of Relative Displacements between Points A and B while Elastic Modulus of Far Field is  $1.0 \times 10^8$  KN/m<sup>2</sup> and Elastic Modulus of Near Field is  $1.0 \times 10^6$  KN/m<sup>2</sup>

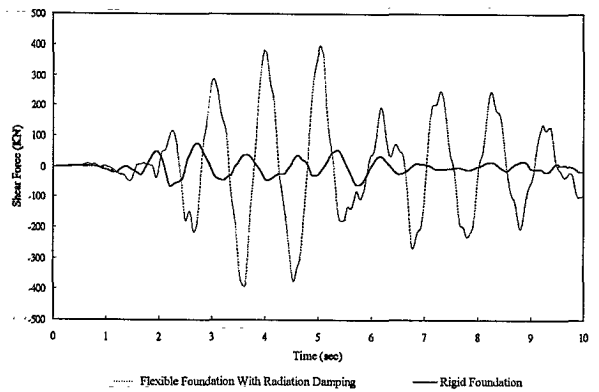


Fig. 11 Comparison of Shear Forces at Point B while Elastic Modulus of Far Field is  $1.0 \times 10^8$  KN/m<sup>2</sup> and Elastic Modulus of Near Field is  $1.0 \times 10^6$  KN/m<sup>2</sup>

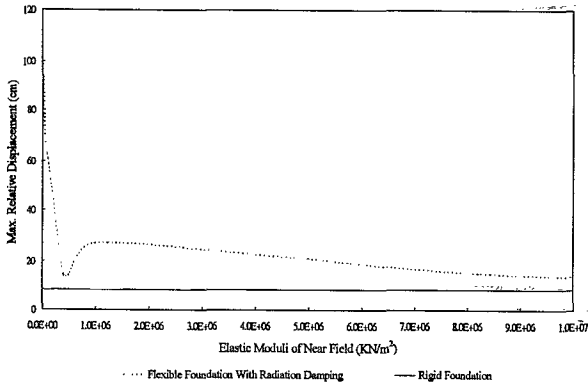


Fig. 12 Comparison of Max. Relative Displacements between Points A and B while Elastic Modulus of Far Field is  $1.0 \times 10^7$  KN/m<sup>2</sup> and Different Elastic Moduli of Near Field are Applied

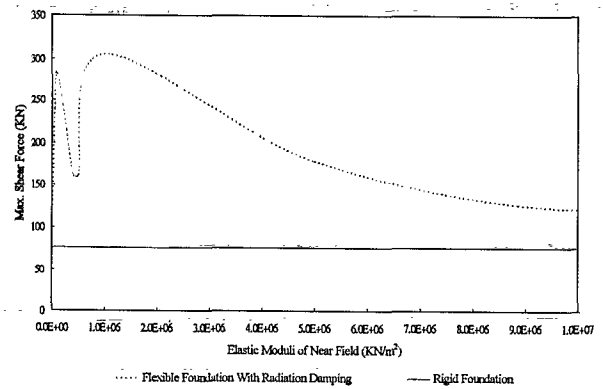


Fig. 14 Comparison of Max. Shear Forces at Point B while Elastic Modulus of Far Field is  $1.0 \times 10^7$  KN/m<sup>2</sup> and Different Elastic Moduli of Near Field are Applied

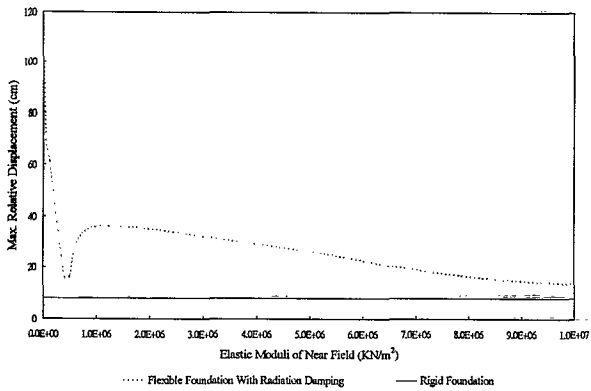


Fig. 13 Comparison of Max. Relative Displacements between Points A and B while Elastic Modulus of Far Field is  $1.0 \times 10^8$  KN/m<sup>2</sup> and Different Elastic Moduli of Near Field are Applied

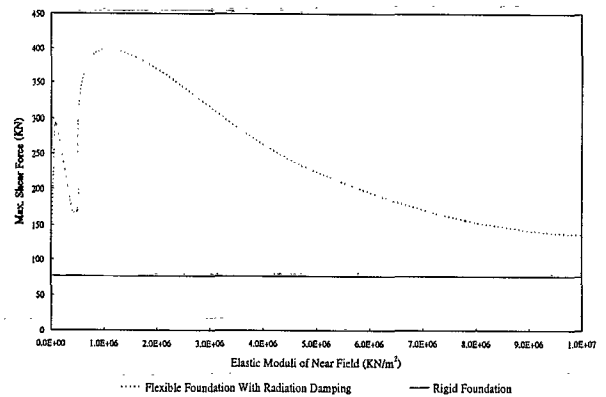


Fig. 15 Comparison of Max. Shear Forces at Point B while Elastic Modulus of Far Field is  $1.0 \times 10^8$  KN/m<sup>2</sup> and Different Elastic Moduli of Near Field are Applied

